

PACS numbers: 42.30.Wb; 87.64.Cc; 87.63.L–; 42.62.Be
DOI: 10.1070/QE2014v044n01ABEH015232

Doppler mapping of an alternating-sign flow with complex geometry using optical coherence tomography

S.G. Proskurin, A.Yu. Potlov, S.V. Frolov

Abstract. **The method of sign-sensitive mapping of the given range of velocities in a flow with complex geometry based on the principles of optical coherence tomography is described. To produce an alternating-sign flow, the 1% aqueous intralipid solution and the tilted capillary entry with the contraction coefficient 4:1 are used. The mapping is controlled using two parameters, the value of one specific velocity (OSV) for mapping and the accuracy of its determination. The structure image and two OSV images (for positive and negative direction of motion) are obtained as a result of selecting and processing the relevant parts of the signal spectrum. The final image is a result of summing these three images and can be used as a Doppler equivelocity contour map.**

Keywords: *Doppler effect, optical coherence tomography, quasi-elastic scattering, flow with complex geometry.*

1. Introduction

Optical coherence tomography (OCT) [1, 2] appeared in late eighties – early nineties of the twentieth century and strongly resembles echographic ultrasonography (US). In contrast to X-ray computed tomography (CT), OCT does not involve the solution of the inverse problem of image reconstruction. In both US and OCT the signal, reflected from the boundaries between tissues having different density (one-dimensional A-scan) is first recorded. The two-dimensional image (B-scan) is obtained as a result of processing and joining several tens or hundreds of thousands of A-scans. In OCT a femtosecond optical pulse of near-IR range is used, which increases the axial spatial resolution by 1–2 orders of magnitude as compared to US ($\Delta z = 1–15$ μm). However, due to strong scattering the depth of coherent probing of a biological object using OCT is reduced to 1–2 mm. Commercial diagnostic OCT instruments have found application in medicine, mainly in ophthalmology (tomography of retina). Retinal tomography appeared to be the only possible method of noninvasive diagnostics of the lateral structure of retina *in vivo* with the resolution of a few micrometres.

By comparing the carrier frequencies of A-scans measured for unmoving and moving surfaces (or liquid flows) one can obtain the Doppler spectra, corresponding to particular flow velocities [3]. One can also measure the phase shift between the sequential or adjacent A-scans, which is often interpreted as a Doppler shift in the phase velocity measurements [4–10]. The first colour US systems were based on the following phase shift encoding: the bluish colours for the motion off the sensor and the reddish colours for the motion towards the sensor.

In this approach the autocorrelation method [10, 11] is used that allows the estimation of the phase shift and its variations. In some sense it is analogous to the particle image velocimetry (PIV), the only difference being that instead of the image shift the recorded quantity is the shift of A-scans or the interferogram phase within their envelopes.

Later the approach to the study of alternating-sign flows of biological fluids, based on positive or negative phase shift of adjacent A-scans, was transferred to the OCT. In this case the Doppler shift f_D is presented neither as the variation of the carrier frequency f_c of the radiation with the centre wavelength λ_0 scattered from the flow moving with the velocity V at the angle α to the optical axis of the probing beam

$$f_D = \pm\frac{V}{\lambda_0}\cos\alpha,$$

nor as the change of the oscillation period $T = 1/f_c$ at sufficiently small velocities:

$$f_D = f_c \pm f_c',$$

where $f_c' = 1/(T \pm \Delta T)$ is the carrier frequency increment and ΔT is the period variation.

Instead, the Doppler shift is determined on the basis of spatially averaged shifts of A-scans within the limits of a running window of the short time Fourier transform (STFT), i.e., the mean phase variation $\overline{\Delta\varphi}$ of the complex signal for a certain number N of sequential A-scans, evaluated using either an autocorrelation or cross-correlation function [5]. Commonly the autocorrelation function originally proposed for US systems is used [10]. In this case,

$$\overline{\Delta\varphi} = -\arctan\left\{\frac{\sum_{m=1}^{N-1}[Q(m)I(m-1) - I(m)Q(m-1)]}{\sum_{m=1}^{N-1}[I(m)I(m-1) - Q(m)Q(m-1)]}\right\}, \quad (1)$$

where m is the A-scan ordinal number; and I and Q are the real and imaginary parts of the complex signal $\Gamma = I + iQ$. Then the Doppler frequency shift is expressed as

$$f_D = \frac{\overline{\Delta\varphi}}{2\pi T_A},$$

S.G. Proskurin, A.Yu. Potlov, S.V. Frolov Tambov State Technical University, ul. Sovetskaya 106, Tambov, 392000, Russia; e-mail: spros@tamb.ru

Received 19 May 2013; revision received 11 October 2013
Kvantovaya Elektronika **44** (1) 54–58 (2014)
Translated by V.L. Derbov

where T_A is the temporal interval between the adjacent A-scans. The flow velocity V is determined by the formula

$$V = \frac{\lambda f}{2n\cos\alpha},$$

where n is the refractive index of the medium.

In Ref. [10] the attention is drawn to the fact that in the methods for studying alternating-sign flows, based on the autocorrelation function (1), the signal-to-noise ratio decreases with increasing axial scanning rate $f_A = 1/T_A$ in the reference arm of the interferometer. That is why for the estimation of the mean phase variation $\overline{\Delta\varphi}$ it is proposed to use the statistical maximum likelihood method (MLM) adapted to OCT, which is less sensitive to the data acquisition rate [10].

The methods described in Refs [4–10] are very sensitive to the motion of surfaces of particles, but possess the 2π phase uncertainty. It the phase shift of one interferogram (A-scan) with respect to the adjacent one attains 2π, then the proportionality of velocity to the phase shift is lost. In the images this phenomenon manifests itself as rings with repeating colours. The procedure of linearization and so called phase unfolding into a single increasing line, the slope of which should correspond to the velocity of motion, cannot fully compensate for this drawback, since it stably works only in some particular cases: for the extremely small concentration of the scatterers or for tremor (vibration of the object as a whole). In this connection, with the aim to remove the abovementioned uncertainty in the US systems, alongside with the sensors necessary to obtain the structure image, specialised Doppler sensors operating at higher frequencies were brought into use [12]. Such sensors are needed for implementing the scheme of recording the Doppler shift in the back-reflected signal.

Analogous sign-sensitive differential (double-beam) optical systems were developed based on the laser sources of continuous high-coherence radiation. With pulsed or low-coherence optical sources such systems are hardly implementable. The synchronisation of the interferometer arm lengths aimed at the localisation of the measured volume in the differential scheme is less stable than in the standard monodyne (single-beam) scheme. However, similar to the structure OCT imaging, it is possible to visualise a single preliminarily chosen velocity in the flow by choosing the transmission band of the filters used in the procedure of processing the interference signal in the frequency domain [13].

It is worth noting that for the time-domain OCT a serious problem is the relatively slow signal pickup and, as a consequence, the artefacts of living object tremor that lead to the blurring of the interference fringes and the reduction of the image definition and contrast.

The aim of the present papers is to implement the sign-sensitive colour mapping of one chosen velocity (OSV) in the flow with complex geometry on the basis of an OCT system with the source of continuous low-coherence IR radiation.

2. Materials and methods

In the experiments the single-beam scheme of recording the Doppler frequency shift of backscattered low-coherence radiation of the superluminescent diode (SLD, Superlum) is used. The control of the experiment, the synchronisation of the scanning process and the signal digitisation are implemented using the PCI unit (National Instruments) and the LabVIEW software package. The algorithm of further processing of the digitised signal is also implemented in this environment [14], and not in the MATLAB package, as in earlier monochrome versions [13]. The use of a single program package allows the operation of the described system in the automated regime and in real time.

The experimental setup (Fig. 1) is based on the scanning Michelson interferometer using single-mode optical waveguides. The tilted capillary entry is used as the object of study [13]. The SLD radiation (λ = 1300 nm, $\Delta\lambda$ = 60 nm) passing through the fibre coupler is directed into the reference arm – the optical delay line (ODL) – and the object arm, i.e., to the object of study. On the way back the radiation from both arms of the interferometer is focused on the detectors, incorporated in the balance scheme. The electric signal is read from the balance detectors, passes through the amplifier and the band-pass filter and is digitised in the time domain by means of a 12-bit ADC. Then the signal is fed into the computer and after the STFT is processed in the frequency domain. As an optical delay line, we used a rapid scanning optical delay (RSOD) with a double pass of the beam, designed on the basis of the diffraction grating and the scanning mirror placed in the focal plane of the focusing lens.

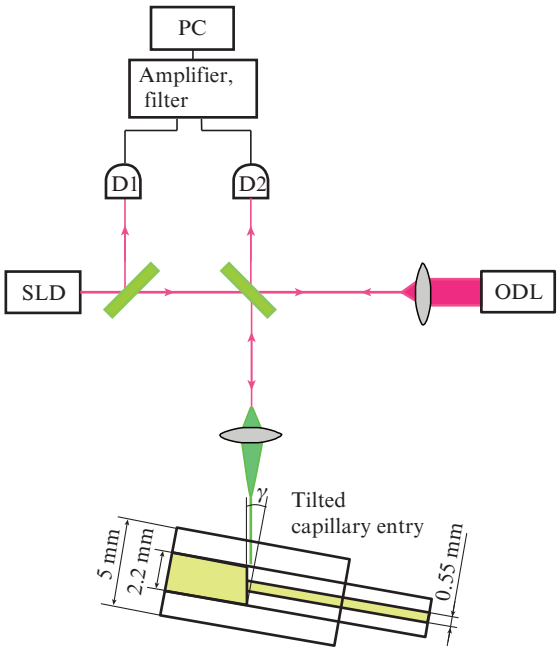

Figure 1. Scheme of the experimental setup: D1, D2 are the detectors, incorporated in the balance scheme; $\gamma = (90° - \alpha)$ is the inclination angle of the capillary entry; the scanning is performed in the plane, perpendicular to the plane of the figure.

Note that in the reference arm one can also use a linearly scanning retroreflector, simultaneously implementing the discrimination with respect to the depth of the studied object and specifying the carrier frequency that appears due to the classical Doppler shift in the process of reflection from the moving mirror. However, increasing the reading rate of A-scans by increasing the velocity of the linearly scanning mirror does not allow decoupling the group and the phase velocity of the signal. The high scanning rate causes not only the high quality of the obtained structure images, but also the

increase in the carrier frequency f_c up to a few megahertz. With such values of f_c it is impossible to detect the Doppler frequency shift having the order of a few kilohertz, corresponding to the velocities of a few millimetres per second. In the described experiment the frequency shift by 1 kHz corresponds to the velocity 2.1 mm s^{-1}.

The use of RSOD allows decoupling the group and the phase velocity and at the sufficiently fast scanning (f_A about a few kilohertz) the shift of the carrier frequency to the range from 20 to 30 kHz. This provides an opportunity to perform the measurements in the region of minimal noise, between the decreasing $1/f$ noise and the white noise, increasing with increasing frequency, as well as to record the Doppler shift of the carrier frequency with good accuracy $\varepsilon \approx 1\% - 5\%$. In this case, in the odd A-scans one always observes a positive shift of the carrier frequency and vice versa. Therefore, by varying the cutting frequencies of the band-pass filter one can determine not only the modulus of the chosen velocity, but also its sign. This will help to divide the B-scan into three parts: the structural image, the map of positive velocities, and the map of negative velocities.

Note that using other fast delay lines one cannot always provide such an opportunity. The spectral domain OCT (SD-OCT) with a fast CCD camera, as well as the laser that allows fast tuning of the radiation wavelength, make it possible to obtain high-quality images in real time [5–8], but their equivalent carrier frequency is very high (~10–100 MHz), and the separation of even and odd A-scans does not lead to the division into positive and negative frequencies. Therefore, in such systems the velocity of the moving object (including its sign) is considered as a characteristic that is directly proportional to the phase shift of the A-scan.

3. Sign-sensitive mapping of the chosen velocity

The specific feature of the proposed mapping method is the possibility of choosing the visualised velocity V_{sel} within the range 0.5 mm $s^{-1} \leqslant V_{sel} \leqslant 500$ mm s^{-1} and the precision of its determination ε within the range $0 \leqslant \varepsilon \leqslant 100\%$. Based on these parameters, the upper V_{upper} and the lower V_{lower} boundaries of the mapped velocity range are expressed as

$$V_{upper} = V_{sel}\left(1 + \frac{\varepsilon}{100\%}\right), \quad V_{lower} = V_{sel}\left(1 - \frac{\varepsilon}{100\%}\right).$$

Thus, the localisation and direction of the flows is mapped not for all velocities, but only for those that fall within the interval of interest $V_{lower} \leqslant V \leqslant V_{upper}$ and the symmetrically located interval $-V_{upper} \leqslant V \leqslant -V_{lower}$.

If the raw data for the colour Doppler mapping are presented in the form of a discrete function $x[k,m]$, where k is the count number within the A-scan, and m is the number of the A-scan itself, then the functions $x_{odd}[k,m]$ and $x_{even}[k,m]$, corresponding to positive and negative shifts of the carrier frequency, are derived from the function $x[k,m]$ as follows:

$$x_{odd}[k,m] = \begin{cases} x[k,m] \text{ for odd } m, \\ 0 \text{ for even } m, \end{cases}$$

$$x_{even}[k,m] = \begin{cases} 0 \text{ for odd } m, \\ x[k,m] \text{ for even } m. \end{cases}$$

For precise detection of OSV within the biological object, for each fixed m the element $x_{odd}[k,m]$ is selected in the given frequency band together with $x_{even}[k,m]$ in the symmetric band by means of fifth-order Bessel digital band-pass filters. The upper ω_{upper} and the lower ω_{lower} cutting frequencies of the band-pass filters are determined as

$$\omega_{upper} = \frac{2\pi f_{st} V_{upper}}{V}, \quad \omega_{lower} = \frac{2\pi f_{st} V_{lower}}{V},$$

where f_{st} is constant for the particular device and represents the Doppler shift, corresponding to $V = 1$ mm s^{-1} and calculated using the following formula:

$$f_{st} = \frac{2V\cos\alpha}{\lambda_0}.$$

Parallel to the above operation, the high- and low-frequency analogue noises are removed from $x[k,m]$ for each fixed m using the third-order Butterworth band-pass filter.

After the digital band-pass filtering the functions $x[k,m]$, $x_{odd}[k,m]$ and $x_{even}[k,m]$ undergo the independent A-scan processing. For each A-scan the fast Fourier transform with the Hemming window is performed. To obtain the spectrogram, the amplitude spectra, calculated within short segments, are joined into a function of two variables. Then, using the Hilbert transform, the envelopes of the demodulated signal are selected, from which a logarithm is taken in order to compress the dynamic range. As a result of these operations, the A-scans become one-dimensional functions again, while their arrays $x[r,m]$, $x_{odd}[r,m]$ and $x_{even}[r,m]$ become full-value two-dimensional B-scans, i.e., structural images, corresponding to the frequency band of the positive part of the Doppler spectrum, selected by the Bessel filter, to the symmetrical frequency band of the negative part of the Doppler spectrum, and to the entire spectrum of the noise-free signal.

The identification of the directions $x_{trends}[r,m]$ of the liquid flow is implemented by the elementwise subtraction of $x_{even}[r,m]$ from $x_{odd}[r,m]$ with the shift by one A-scan:

$$x_{odd-1}[r,m] = x_{odd}[r,m] \backslash x_{odd}[r,m_{last}],$$

$$x_{trends}[r,m] = x_{odd-1}[r,m+1] \backslash x_{even}[r,m],$$

where the symbol '\' stands for the difference of functions $x_{odd}[r,m]$ and $x_{odd}[r,m_{last}]$ considered as two sets, and m_{last} is the number of the last A-scan. Then, using the logical analysis of the obtained results, the functions are constructed that characterise the positively, $x_{pos}[r,m]$, and negatively, $x_{neg}[r,m]$, directed flows:

$$x_{pos}[r,m] = x_{trends}[r,m]h(x_{trends}[r,m]),$$

$$x_{neg}[r,m] = x_{trends}[r,m]h(-x_{trends}[r,m]),$$

where $h(x)$ is the Heaviside function.

It is important to note that the unmoving part of the signal (i.e., the part, recorded at the carrier frequency) will be most probably not present in $x_{pos}[r,m]$ and $x_{neg}[r,m]$; therefore, the formulae for identifying the liquid flow directions are used in order to account for the case, when the scanning velocity in the object arm falls within the chosen range of the detected flow velocities.

The encoding of the functions $x_{pos}[r,m]$ and $x_{neg}[r,m]$ is performed using the formulae:

$$x_{mpos}[r,m] = h(x_{pos}[r,m] - P),$$

$$x_{\text{mneg}}[r,m] = \overline{-h(x_{\text{neg}}[r,m] + P)},$$

where P is the experimentally found minimal level, separating the flow signal from the noise. Then $x_{\text{mpos}}[r,m]$ and $x_{\text{mneg}}[r,m]$ are integrated into the image $x_{\text{im}}[r,m]$ of flow directions and locations

$$x_{\text{im}}[r,m] = x_{\text{mpos}}[r,m] + x_{\text{mneg}}[r,m].$$

Then $x[r,m]$ is transformed into the special colour scale. The obtained B-scan $x_{\text{st}}[r,m]$ is joined with the image of directions and localisation of flows $x_{\text{im}}[r,m]$ to form the summary function $x_{\text{sum}}[r,m]$:

$$x_{\text{sum}}[r,m] = x_{\text{st}}[r,m] + x_{\text{im}}[r,m].$$

Finally, to construct the general picture on the basis of the function $x_{\text{sum}}[r,m]$ the pseudo-colour scale is used that comprises green tints for visualisation of the inner structure of the unmoving object, red and blue colours for visualisation of movement directions, and white colour as the reference point (neither motion, nor reflection).

4. Results and discussion

The described algorithm was implemented as a special-purpose software product using the graphical programming language G in the LabVIEW software package [14].

To test and debug the programme we used the simplest hydrodynamical model of the Newtonian liquid flow. This model is a transparent tube with the inner diameter of 0.55 mm. Instead of blood we used the 1% aqueous solution of intralipid. Figure 2 shows the structure image, obtained as a result of scanning of this model, the OSV-image, and the final image.

The carrier frequency of the interference signal and the cutting frequencies of the band-pass filters were chosen such that both the unmoving wall and the flow velocity $V_{\text{sel}} = 7$ mm s^{-1} (with the precision $\varepsilon \approx 9\%$) could be imaged.

Figure 3 shows the results of the experiments with the tilted capillary entry (see Fig. 1, the object of study is located in the object arm) that allows the formation of an alternating-sign flow with complex geometry [13]. The scanning was performed within the plane, perpendicular to the plane of the figure (see Fig. 1) at the distance 1 mm from the tilted capillary entry. The detected signal contains the information about the unmoving walls, as well as about the positively and negatively directed flows (bright stripes in Fig. 3a). However, their visual separation is not possible. The developed algorithm makes this separation possible in real time. The chosen value of the mapped velocity equals 6 mm s^{-1} ($\varepsilon \approx 26\%$).

Note that the choice of the filter transmission bandwidth allows the control of the velocity separation accuracy, while the choice of the mean frequency of the filter provides the Doppler mapping for the particular velocity under study. In this case there is no qualitative encoding by the tints of red or blue, the velocity is determined quantitatively with the given accuracy, and the colour characterises the direction only. This opens the possibility to use the black-and-white representation of the OSV-maps as well, provided that the velocity value, its accuracy and sign are specified.

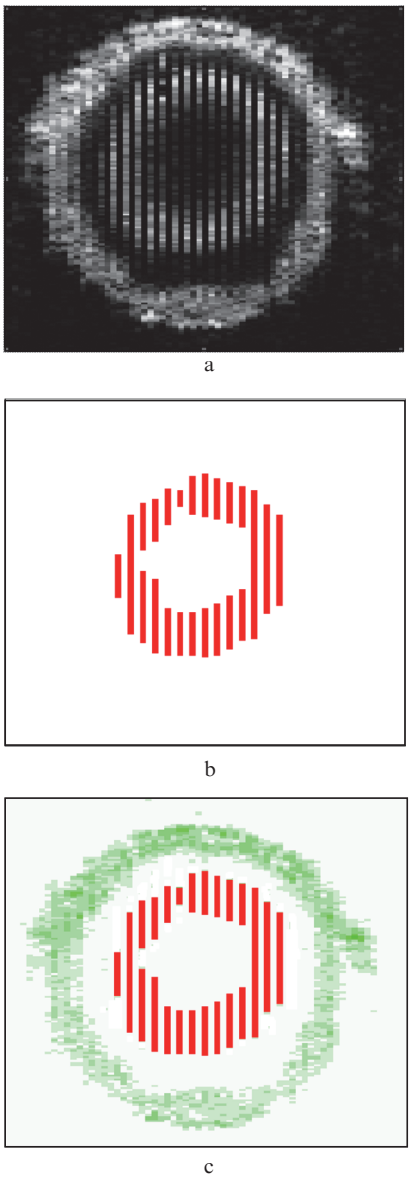

Figure 2. (a) Structural image, (b) OSV-image and (c) the final image for the cylindrical capillary.

5. Conclusions

In the present paper we report the development and application of the method of Doppler colour mapping of one previously chosen velocity in a turbulent flow, based on low-coherence methods of spatial discrimination of the optical signal. The proposed method is implemented in the form of the software product that allows the mapping in the automated regime of the OCT system interference signal processing. The raw data are separated into three parts, corresponding to the unmoving object, the positively and negatively directed flows. The further independent signal processing procedure yields the structure image and two images of the chosen velocity, which are then normalised, encoded and joined. In application to biological objects (blood vessels and vascular branching, heart) this method makes it possible to obtain in real time the anatomical maps of the chosen velocities in the normal and pathological state. The described algorithm can be also applied not only in optical, but also in ultrasonic systems.

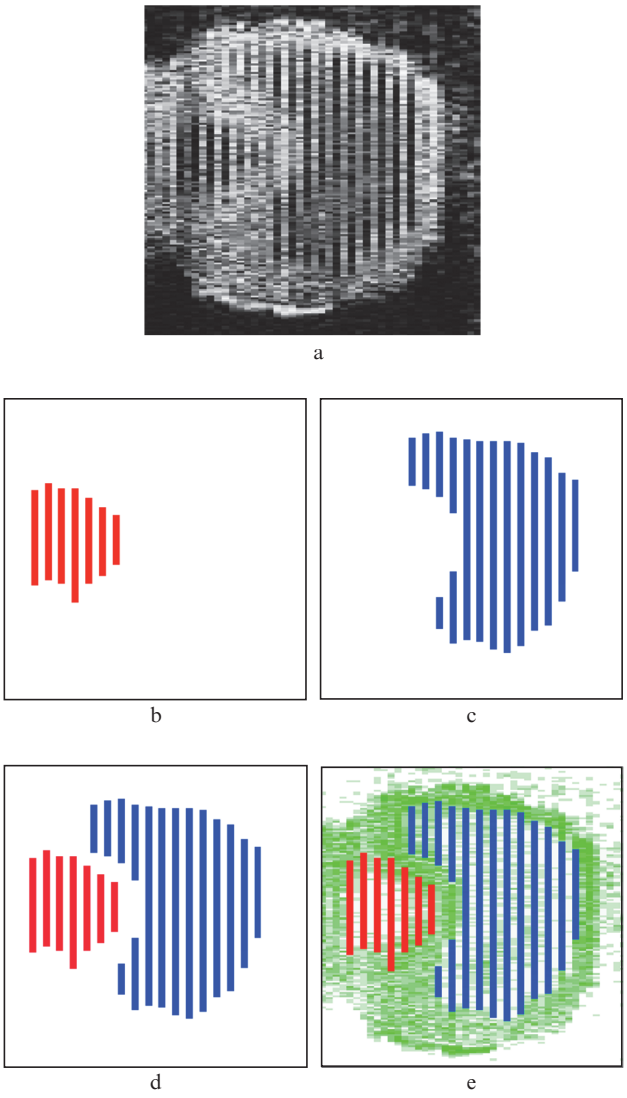

Figure 3. (a) Structural image, OSV-image of the motion (b) towards the detector and (c) off the detector, (d) alternating-sign OSV-image and (e) the resulting image for the flow possessing complex geometry.

Acknowledgements. The present work was supported by the State Contract Nos 9576p/14219 and 10741p/16955 of the U.M.N.I.K. Programme.

References

1. Zimnyakov D.A., Tuchin V.V. *Kvantovaya Elektron.*, **32** (10), 849 (2002) [*Quantum Electron.*, **32** (10), 849 (2002)].
2. Gladkova N.D. *Opticheskaya kogerentnaya tomografiya v ryadu metodov meditsinskoy vizualizatsii. Kurs lektsii* (Optical Coherence Tomography among the Methods of Medical Visualisation. A Lecture Course) (Nizhny Novgorod: Institute of Applied Physics RAS Publishers, 2005).
3. Chen Z., Milner T.E., Dave D., Nelson J.S. *Opt. Lett.*, **22** (1), 64 (1997).
4. Ding Z., Zhao Y., Ren H., Nelson J., Chen Z. *Opt. Express*, **10** (5), 236 (2002).
5. Wang L., Wang Y., Guo S., Zhang J., Bachman M., Li G., Chen Z. *Opt. Commun.*, **242**, 345 (2004).
6. Yang V., Gordon M., Mok A., Zhao Y., Chen Z., Cobbold R., Wilson B., Alex V. *Opt. Commun.*, **208**, 209 (2002).
7. White B.R., Pierce M.C., Nassif N., Cense B., Park B.H., Tearney G.J., Bouma B.E., Chen T.C., de Boer J.F. *Opt. Express*, **11** (25), 3490 (2003).
8. Motaghiannezam S., Koos D., Fraser S. *J. Biomed. Opt.*, **17** (2), 026011 (2012).
9. Chan A., Lam E., Srinivasan V. *IEEE Trans. Med. Imaging*, **32** (6), 1033 (2013).
10. Kasai C., Namekawa K., Koyano A., Omoto R. *IEEE Trans. Son. Ultrason.*, **32** (3), 458 (1985).
11. Doronin A., Meglinski I. *Laser Photonics Rev.*, **7** (1), 797 (2013).
12. Saitoh S., Izumi M., Mine Y. *IEEE Trans. Ultrason. Ferroelectr. Freq. Control*, **42** (2), 294 (1995).
13. Proskurin S.G., Wang R.K. *Proc. SPIE Int. Soc. Opt. Eng.*, **5696**, 129 (2005).
14. Proskurin S.G., Potlov A.Yu., Frolov S.V. Certificate of State Registration of Computer Program, Federal Institute of Industrial Property, No. 2013614222 (2013).